Novel polarization insensitive 40-channels 100 GHz spacing fold-back planar Echelle grating mux/demux for photonic integrated wavelength selective switches

YU WANG, NICOLA CALABRETTA

ECO Group, Eindhoven Hendrik Casimir Institute, Eindhoven University of Technology, 5612 AZ Eindhoven, The Netherlands
**Corresponding author: y.wang13@tue.nl*

Received XX Month XXXX; revised XX Month, XXXX; accepted XX Month XXXX; posted XX Month XXXX (Doc. ID XXXXX); published XX Month

We present and numerically demonstrate a novel polarization insensitive (PI) 40-channels 100 GHz spacing fold-back planar Echelle grating (PEG) multiplexers/ demultiplexers (Mux/Demux) to realize the compact 1×2 crossing-less photonic integrated wavelength selective switch (PIC-WSS). The PI operation is achieved by a polarization splitter to feed the TE mode and TM mode into the PEG via two waveguides with different incidental angles so that the diffracted optical signals (two different modes) combine at the same PEG's output waveguide. By optimizing the design of the different inputs/outputs angles combinations and sharing the same blazed angle, a single compact PI PEG with fold-back configuration can simultaneously work as twice Demuxes and twice Muxes. The single fold-back PI PEG's footprint including input/output waveguides is only ~ 40 mm². The numerical results show that 40-channels 100 GHz spaced PI fold-back PEG owns < 2.4 dB insertion loss, <-60 dB cross-talk, zero polarization dependent wavelength shift (PDWS), 0.3 dB polarization dependent loss (PDL), < 0.5 dB loss variation and < 0.01 nm wavelength shift between Mux and Demux. © 2022 Optica Publishing Group

Many advanced applications like 5G, edge cloud services and internet of things steadily boost the growth of data traffic in metro networks. Innovative programmable metro network sub-systems are required to efficiently switch and route the large, heterogeneous, and dynamic data traffics. PIC-WSSs are promising and efficient solutions to implement a programmable network by routing wavelengths from any inputs to any outputs without E/O/E conversion [1,2]. The PIC-WSS has the potential to provide optical switching with compact footprint, high stability, low cost, and low power consumption. Reported 1×N PIC-WSSs have a configuration consisting of integrated Mux/Demux for the wavelength separation/combiner, broadcast splitters and many waveguide crossings, and photonic switches/gates for wavelength bypass/dropping/ blocking (see the configuration in Fig. 1 (a)) [3]. The conventional photonic integrated Mux/Demux in PIC-WSSs employ arrayed waveguide grating (AWG) on different photonic platforms. In [4], we have demonstrated a hybrid integrated WSS consisting of InP semiconductor optical amplifiers (SOAs) as optical gates with nanoseconds switching operation and two silicon AWGs (one for Mux and the other for Demux), but limited to 12-channels AWG and requires wavelength registration to match the central wavelengths of the two AWGs. Another 40-channels 100 GHz spaced PIC-WSS approach on silica platform [5] exploited a single AWG in a fold-back configuration as both a Mux and a Demux to eliminate the wavelength mismatch, but at the cost of larger chip size (~11000 mm²) and higher losses/cross-talks due to numerous waveguides crossing. Fold-back PEG is an alternative solution to the fold-back AWG as the PEG can provide smaller footprint to implement an ultra-compact PIC-WSS design by reusing the free propagation region (FPR) and the grating facets for implementing

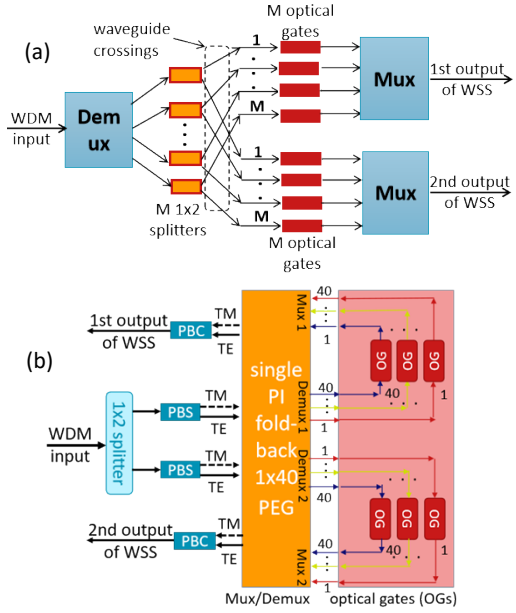

Fig. 1. (a) schematic of conventional 1×2 M-channels WSS with separate Mux/Demux. (b) schematic of 1×2 40-channels crossing-less PI WSS employing single PI fold-back PEG, PBS, polarization beam combiner (PBC) and optical gates (OGs).

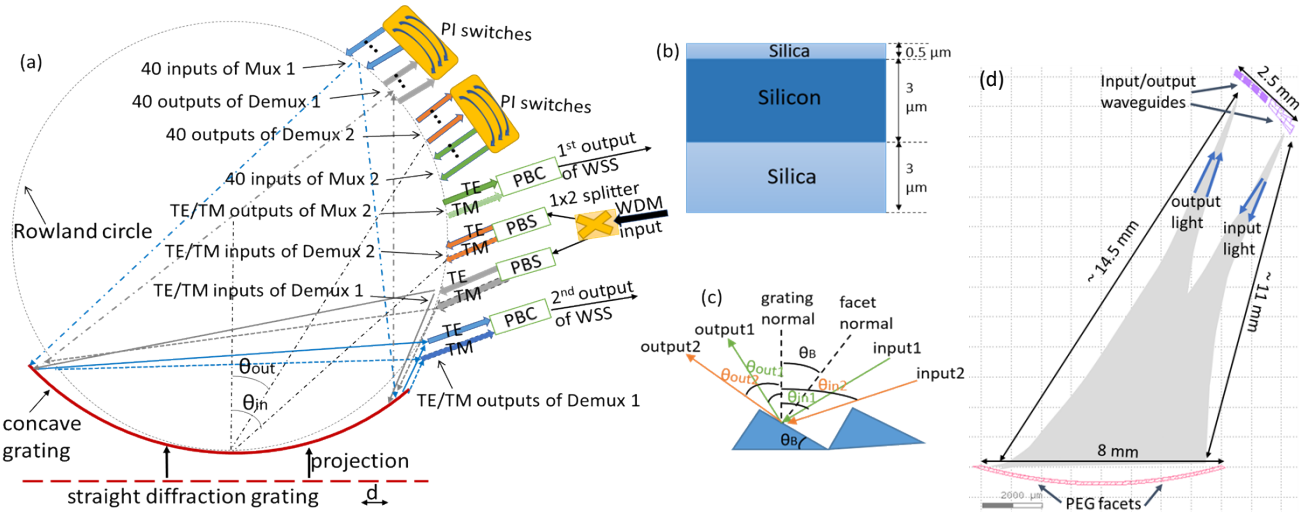

Fig. 2. (a) structure of PI fold-back PEG (twice Demuxes and twice Muxes) combining PBS and PBC for 1×2 crossing-less WSS. (b) structure of 3-μm silicon slab waveguide. (c) blazed angle for two input/output combinations. (d) layout of the 1×40 PEG (grey part: area of light transmission).

simultaneously multiple Muxes/Demuxes within the same photonic circuit. However, for a practical implementation of a PI PIC-WSS, also the PEG should have PI operation. Several methods were proposed to design PI PEG. In [6], the two polarization states (TE and TM) were separated by the Bragg grating and demultiplexed by two different PEGs to achieve polarization insensitivity, but two PEGs could lead to wavelength mismatch and thus high insertion losses. In [7], the PDWS is compensated with an extra-etching in the FPR, but the second lithography step increases fabrication complexity and brings extra insertion loss as well as the edge channels' high PDWS (0.15 nm).

In this paper, we present and numerically demonstrate, for the first time to the best of our knowledge, a 40-channels 100 GHz spaced PI PEG with fold-back configuration that can simultaneously work as multiple Muxes/Demuxes for compact and crossing-less 1×2 PI PIC-WSS design. By employing a 1×2 splitter to divide the input WDM data and two polarization beam splitters (PBSs) to feed two polarization states into different input waveguides with different angles (see the configuration in Fig.1 (b) and Fig. 2 (a)), the single PI PEG with folded configuration prevents waveguides crossing to achieve low cross-talk and low insertion loss as well as negligible PDL and PDWS. Numerical results show that for all PEG's channels of the two Muxes and two Demuxes the insertion losses are 1.5 dB ~ 2.1 dB for TE and 1.8 dB ~ 2.4 dB for TM, the cross-talk levels are better than -60 dB, the PDL is less than 0.3 dB, the PDWS is zero at central channel, 0.01 nm channel wavelength shift and < 0.5 dB loss variation between Mux and Demux.

The schematic of the PI fold-back PEG is shown in Fig. 2 (a). The operation principle of the PI fold-back PEG based 1×2 crossing-less WSS is explained as follows. The optical power of the input WDM channels with 100 GHz spacing is first split by a 50:50 power splitter to generate two copies of the input WDM channels. Each copy of the input WDM channels is fed into a PBS to separate the TE and TM modes. Then the TE mode and TM mode of the first copy (second copy) are launched into the TE input and TM input of Demux 1 (inputs of Demux 2), respectively. The launching input angle of the TE and TM modes and the PEG are designed so that the 40 TE and TM channels diffracted by the PEG grating are demultiplexed and then combined to the same 40 outputs waveguides of Demux 1 (outputs of Demux 2). The separated 40 channels are switched by the optical PI switch array and then guided back to the 40 inputs of Mux 1 (inputs of Mux 2). The switched channels are multiplexed to the TE and TM output port of Mux 1 (outputs of Mux 2). The two polarizations are combined by the PBC to the first (second) output of the WSS. By programming the switch gates, any wavelength can be switched/multi-casted to the two WSS output ports.

The detailed method for PI and fold-back design is described as follows. The concaved PEG is the projection of the straight diffraction grating on the waveguide plane. The input and output waveguides are placed on the imaginary Rowland circle (RC) with radius R. The multi-wavelengths beam, injected from the input waveguides diverges in the FPR. Then the diffracted light beam, reflected by the grating facets, focuses to the output waveguides on the RC. Due to different refractive index and phase paths, different wavelengths are separated to different output ports. The relationship between the positions of incident light (input waveguide) and diffracted light (output waveguide) are determined by the diffraction equation [8,9]:

$$d\left(\sin(\theta_{in}) + \sin(\theta_{out})\right) = (m\lambda)/n \qquad (1)$$

where d is the grating facet period, θ_{in} is the incident angle of light, θ_{out} is the output angle of diffracted light, m is the diffraction order, λ is the incident wavelength value in the free space, and n is the effective refractive index of λ in the FPR. For the fixed input angle and grating period, the output angle of TE and TM modes are:

$$\theta_{out}^{TE} = \arcsin\left(\frac{m\lambda}{dn_{TE}} - \sin(\theta_{in})\right) \qquad (2)$$

$$\theta_{out}^{TM} = \arcsin\left(\frac{m\lambda}{dn_{TM}} - \sin(\theta_{in})\right) \qquad (3)$$

As TE and TM have different effective refractive indexes in the FPR, the output angle is different for TE and TM, which leads to PDL and PDWS. To achieve the PI operation, both TE and TM signals should be directed to the same output waveguide. Therefore, we fix the output waveguide position ($\theta_{out}^{TM} = \theta_{out}^{TE} = \theta_{out}$), and design the input waveguides for TE input and TM input at different incident angles to diffract the two polarizations to the same output port. The design strategy is first to fix the diffraction order m and central wavelength λ, then choose the input/output angle of the TE mode (θ_{in}^{TE} and θ_{out}). The grating period is calculated by:

$$d = (m\lambda)/\left(n_{TE}(\sin(\theta_{out}) + \sin\left(\theta_{in}^{TE}\right))\right) \qquad (4)$$

As the output angle of TM and TE should be the same, the input angle for TM mode is calculated by:

$$\theta_{in}^{TM} = \arcsin\left((m\lambda)/(n_{TM}d) - \sin(\theta_{out})\right) \quad (5)$$

And the physical spacing between the input TE and input TM waveguides is:

$$\Delta s = 4\pi R(\theta_{in}^{TE} - \theta_{in}^{TM}) \quad (6)$$

By setting the different input angles for TE and TM, the two modes can be diffracted and reflected to the same output waveguides without PDWS and PDL.

In our design, the 3-μm thick silicon (waveguide core) on silica (substrate) platform is employed as the slab waveguide for guiding light (see Fig. 2 (b)) [10]. The grating facets are coated by gold for reflection. The effective refractive index of TE and TM (n_{TE} and n_{TM}) at central wavelength of 1547.72 nm in the FPR are 3.4672 and 3.4664, respectively. The diffraction order m is set to 6 for both TE and TM, which results in ~258 nm free spectrum range (FSR). For TE mode, the input angle is set to 27° with output angle of 20°, and the grating period d is calculated to 3.36 μm. For TM mode, the input angle is 27.01° which results in an output angle of 20° (same as for TE). The physical distance of TE and TM input is ~ 3 μm.

To achieve maximum diffraction efficiency and minimum insertion loss, the grating facet is designed with blazed angle (θ_B), which ensures the direction of the reflected light to be the same as zeroth diffraction's [8][9]:

$$\theta_B = (\theta_{in} + \theta_{out})/2 \quad (7)$$

If the different combinations of input and output angles satisfy the same blazed angle condition (such as $(\theta_{in}^1 + \theta_{out}^1)/2 = (\theta_{in}^2 + \theta_{out}^2)/2 = \theta_B$), namely, share the same blazed angle, the same blazed grating can provide maximum diffraction efficiency for the different light beams injected from different input angles (see Fig. 2 (c)). The first input/output combination of TE mode ($(\theta_{in}^{TE1} + \theta_{out}^{TE1})$) defines the grating period (see equation (4)). Then the input angle of the other combination is set to θ_{in}^{TEn} following the rules in [9], and the corresponding output angle is calculated by:

$$\theta_{out}^{TEn} = \arcsin\left((m\lambda)/(n_{TE}d) - \sin(\theta_{in}^{TEn})\right) \quad (8)$$

In order to achieve the PI operation, the output angle of TM mode is set to the same value as θ_{out}^{TEn}, and the input angle of TM (θ_{in}^{TMn}) is calculated by equation (5). To reuse the single PEG four times for twice multiplexing and twice demultiplexing, our fold-back PEG is designed with four input/output angles combinations. The first input/output combination for TE mode is set to 27° and 20°, resulting 23.5° blazed angle, and the other three combinations for TE are 28.5°/18.59°, 25.5°/21.44° and 24°/22.91°. For TM mode, the four combinations are 27.01°/20°, 28.51°/18.59°, 25.51°/21.44° and 24.01°/22.91°, respectively. Since the grating period d is fixed and calculated by the first input/output combination, the other combination has a slight deviation compared with the blazed angle of 23.5°, which will result in extra negligible loss. By reusing the same PEG and sharing the same blazed angle, the fold-back configuration ensures zero wavelength shift between different input/output groups. Benefiting from the PEG's bidirectionality, the input and output can be swapped, namely, the light beams launched from the output waveguides can also be diffracted and reflected to the input waveguide. For the 1×2 WSS configuration, the single PEG works as twice Demux and twice Mux. The Demux 1 uses angle combination of 27° TE mode input, 27.01° TM mode input and 20° same output for two modes. The Mux 1 employs 18.59° same input for TE and TM, 28.5° TE output and 28.51° TM output. For Demux 2, the waveguide positions are set with 25.5° TE input, 25.51° TM input and 21.44° same output. The Mux 2 owns 22.91° input, 24° TE output and 24.01° TM output. The main design parameters are summarized in Table 1. The single fold-back PEG's size including grating facets and area of light transmission is only ~ 40 mm² (see the layout in Fig. 2 (d)), which is much smaller than the AWGs in [4] and [5].

Table 1. Main design parameters of PI fold-back PEG

Grating period	3.36 μm	Grating length	8000 μm
Diffraction order	6	Rowland radius	7500 μm
Central wavelength	1547.72 nm	Distance of TE/TM input	3 μm
Channel number	40	Input/output angle of deMux1	27°/20° (TE) 27.01°/20° (TM)
Blazed angle	23.5°	Input/output angle of Mux1	28.5°/18.59° (TE) 28.51°/18.59° (TM)
Channel spacing	100 GHz	Input/output angle of deMux2	25.5°/21.44° (TE) 25.51°/21.44° (TM)
FSR	~258 nm	Input/output angle of Mux2	24°/22.91°(TE) 24.01°/22.91° (TM)

The software Epipprop is used as the simulator. The 100 GHz spaced 40-channels simulated output spectra and magnified spectra of Demux 1, Mux 1, Demux 2 and Mux 2 are illustrated in Fig.

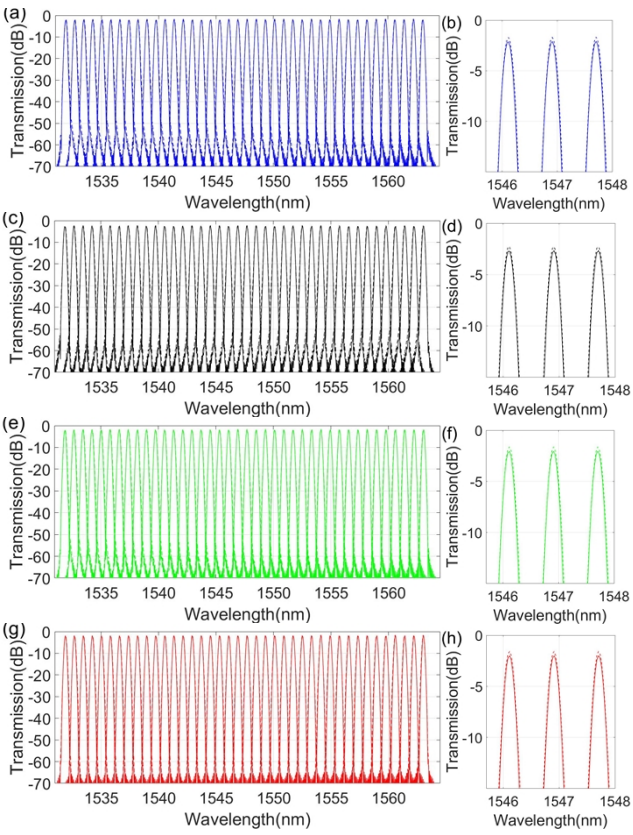

Fig. 3. Output spectra with TE mode (solid curve) and TM mode (dashed curve) of deMux 1 (a), Mux 1 (c), deMux 2 (e) and Mux 2 (g); magnified spectra at central channels of deMux 1 (b), Mux 1 (d), deMux 2 (f) and Mux 2 (h).

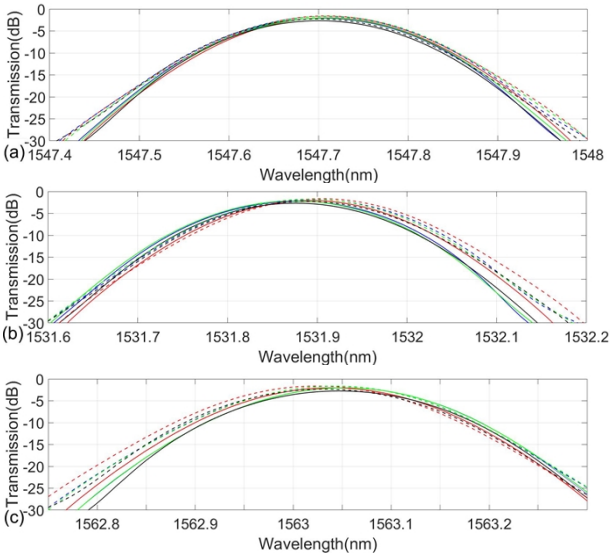

Fig. 4. Detailed output spectra at 1547.72 nm (a), 1531.90 nm (b) and 1563.86 nm (c) of Demux 1 (blue curve), Mux 1 (black curve), Demux 2 (green curve) and Mux 2 (red curve) with TE mode (solid curve) and TM mode (dashed curve).

3 (a) to (h), respectively. Fig. 4 (a), (b) and (c) show the overlapped detailed spectra of two Demuxes and two Muxes at central wavelength (1547.72 nm) and C-band edge wavelengths (1531.90 nm and 1563.86 nm), respectively. The results show that from 1530 nm to 1565 nm for all Demuxes and Muxes, insertion losses range from 1.5 dB to 2.1 dB for TM mode and from 1.8 dB to 2.4 dB for TE mode. The PDWS at central channel is zero, and is 0.009 nm at edge channel, which is smaller than [6] (~ 0.02 nm) and [7] (0.15 nm). All channels have ~ 0.3 dB PDL, which is caused by polarization dependent reflective coating and could be eliminated by removing metal coating from the grating's nonreflecting facets [11]. The cross-talk levels are around -60 dB in average for all 40 channels. The loss variation of 0.04 dB to 0.5 dB between demultiplexing and multiplexing is observed due to slight deviation from blazed angle. The wavelength mismatching between Demux and Mux is zero at central channel and 0.01 nm at edge channel. All simulated results are summarized in Table 2. The effect of TE/TM input distance variation on PI performance has also been studied by simulating TM spectrum with distance variation till ±200 nm with 50 nm step (see Fig. 5). The variation of ± 200 nm only result in 0.02 nm PDWS and 0.4 dB PDL. The fabrication tolerance could be further reduced by increasing RC' radius, namely, the distance of TE and TM input. The typical refractive index variation after fabrication is in the order of ~ 1×10^{-5} that leads to ~ 0.005 nm central wavelength shift for both TE mode and TM mode. When the variation of blazed angle is < 1°, the increase of insertion loss is < 0.7 dB and the increase of cross-talk is < 5 dB.

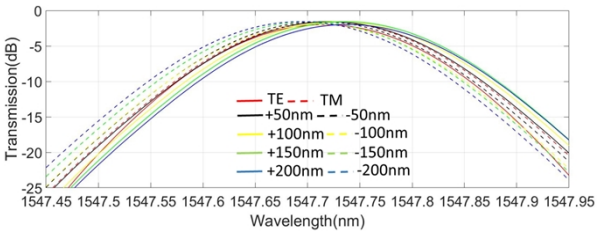

Fig. 5. Detailed output spectra of original TE/TM design, and TM with distance variation of ±50nm, ±100nm, ±150nm and ±200nm.

Table 2. Simulated results of the PI fold-back PEG

	Demux 1	Mux 1	Demux 2	Mux 2
Insertion losses (dB) (TE)	2.0 ~ 2.1	2.3 ~ 2.4	1.9 ~ 2.0	1.8 ~ 1.9
Insertion losses (dB) (TM)	1.7 ~ 1.8	2.0 ~ 2.1	1.6 ~ 1.7	1.5 ~ 1.6
PDL (dB)	~ 0.3	~ 0.3	~ 0.3	~ 0.3
Loss variation (dB)	0.04 ~ 0.5	PDWS (nm)		0 ~ 0.009
Wavelength mismatching (nm)	0 ~ 0.01	Cross-talk (dB)		-60

In summary, we designed and numerically demonstrated a novel PI fold-back PEG serving simultaneously as twice the Demux and Mux required in a PI PIC-WSS. The single PI fold-back PEG owns 40 channels and 100 GHz spacing for Mux/Demux with low insertion loss of 1.5 dB ~ 2.4 dB, 0 ~ 0.009 nm PDWS, ~ 0.3 dB PDL, low cross-talk < -60 dB, 0.04 dB ~ 0.5 dB loss variation and 0 ~ 0.01 nm wavelength mismatching between Muxes and Demuxes, and compact footprint of ~ 40 mm^2. The flat-top response of the PEG can be achieved by placing an MMI in front of the input waveguide [9], which will be considered in future work. The PI fold-back concept can be in principle extended to PI N-use fold-back PEG for larger port ultra-compact crossing-less PI PIC-WSS.

Funding. European Union's Horizon 2020 research and innovation programme under the Marie Skłodowska-Curie grant agreement 814276.

Disclosures. The authors declare no conflicts of interest.

Data Availability. Data underlying the results presented in this paper are not publicly available at this time but may be obtained from the authors upon reasonable request.

References

1. N. Calabretta, N. Tessema, K. Prifti, A. Rasoulzadehzali, Y. Wang, S. Bhat, G. Delrosso, T. Aalto, and R. Stabile, Proc. SPIE 11690, Smart Photonic and Optoelectronic Integrated Circuits XXIII, 116900O (2021).
2. Y. Wang, J. Shin, N. Tessema, M. Hout, S. Heide, C. Okonkwo, H. Jung, and N. Calabretta, Opt. Lett. 46, 5324-5327 (2021).
3. F. Testa, S. Tondini, F. Gambini, P. Velha, A. Bianchi, C. Kopp, M. Hofbauer, C. L. Manganelli, N. Zecevic, S. Faralli, G. Pares, R. Enne, A. Serrano, B. Goll, G. Fontana, A. Chalyan, J. -M. Lee, P. Pintus, G. Chiaretti, H. Zimmermann, L. Pavesi, C. J. Oton, and S. Stracca, Journal of Lightwave Technology, vol. 37, no. 2, pp. 345-355, 2019.
4. N. Tessema, G. Delrosso, S. Bhat, K. Prifti, A. Rasoulzadehzali, Y. Wang, T. Aalto, R. Stabile, and N. Calabretta, 2021 International Conference on Optical Network Design and Modeling (ONDM), pp. 1-5, 2021.
5. T. Yoshida, H. Asakura, T. Mizuno, H. Takahashi, and H. Tsuda, 39th European Conference and Exhibition on Optical Communication (ECOC 2013), pp. 1-3, 2013.
6. Ning Zhu, Opt. Lett. 35, 1599-1601 (2010).
7. N. Zhu, J. Song, L. Wosinski and S. He, IEEE Photonics Technology Letters, vol. 20, no. 10, pp. 860-862, 2008.
8. Calvo, M.L., & Lakshminarayanan, V. (2007). Optical Waveguides: From Theory to Applied Technologies (1st ed.). CRC Press.
9. R. J. Lycett, D. F. G. Gallagher, and V. J. Brulis, IEEE Photonics Journal, vol. 5, no. 2, pp. 2400123-2400123, April 2013.
10. T. Aalto, M. Harjanne, and M. Cherchi, Proc. SPIE 9891, Silicon Photonics and Photonic Integrated Circuits V, 98911G (2016).
11. Janz, A. Balakrishnan, S. Charbonneau, P. Cheben, M. Cloutier, A. Delâge, K. Dossou, L. Erickson, M. Gao, P. A. Krug, B. Lamontagne, M. Packirisami, M. Pearson, and D.-X. Xu, IEEE Photonics Technol. Lett. 16, 503 (2004).

References

1. N. Calabretta, N. Tessema, K. Prifti, A. Rasoulzadehzali, Yu Wang, S. Bhat, G. Delrosso, T. Aalto, and R. Stabile, "Programmable modular photonic integrated switches for beyond 5G metro optical networks," Proc. SPIE 11690, Smart Photonic and Optoelectronic Integrated Circuits XXIII, 116900O (5 March 2021); https://doi.org/10.1117/12.2580374
2. Yu Wang, Jang-Uk Shin, Netsanet Tessema, Menno van den Hout, Sjoerd van der Heide, Chigo Okonkwo, Hyun-Do Jung, and Nicola Calabretta, "Ultra-wide band (O to L) photonic integrated polymer cross-bar switch matrix," Opt. Lett. 46, 5324-5327 (2021); https://doi.org/10.1364/OL.437898
3. F. Testa, S. Tondini, F. Gambini, P. Velha, A. Bianchi, C. Kopp, M. Hofbauer, C. L. Manganelli, N. Zecevic, S. Faralli, G. Pares, R. Enne, A. Serrano, B. Goll, G. Fontana, A. Chalyan, J. -M. Lee, P. Pintus, G. Chiaretti, H. Zimmermann, L. Pavesi, C. J. Oton, and S. Stracca, "Integrated Reconfigurable Silicon Photonics Switch Matrix in IRIS Project: Technological Achievements and Experimental Results," in Journal of Lightwave Technology, vol. 37, no. 2, pp. 345-355, 15 Jan.15, 2019, doi: 10.1109/JLT.2018.2871974.
4. N. Tessema, G. Delrosso, S. Bhat, K. Prifti, A. Rasoulzadehzali, Y. Wang, T. Aalto, R. Stabile, and N. Calabretta, "Wavelength selective photonic integrated switches for ROADM node functionality in ultrahigh capacity metro network," 2021 International Conference on Optical Network Design and Modeling (ONDM), 2021, pp. 1-5, doi: 10.23919/ONDM51796.2021.9492447.
5. T. Yoshida, H. Asakura, T. Mizuno, H. Takahashi, and H. Tsuda, "Silica-based 100-GHz-spacing integrated 40-λ 1×4 wavelength selective switch," 39th European Conference and Exhibition on Optical Communication (ECOC 2013), 2013, pp. 1-3, doi: 10.1049/cp.2013.1473.
6. Ning Zhu, "Proposal of a polarization-insensitive echelle grating demultiplexer based on a nanophotonic silicon-on-insulator platform through a dual-grating system," Opt. Lett. 35, 1599-1601 (2010)
7. N. Zhu, J. Song, L. Wosinski, and S. He, "Design of a Polarization-Insensitive Echelle Grating Demultiplexer Based on Silicon Nanophotonic Wires," in IEEE Photonics Technology Letters, vol. 20, no. 10, pp. 860-862, May15, 2008, doi: 10.1109/LPT.2008.921839.
8. Calvo, M.L., & Lakshminarayanan, V. (2007). Optical Waveguides: From Theory to Applied Technologies (1st ed.). CRC Press. https://doi.org/10.1201/9781315221342
9. Lycett, R.J., Gallagher, D.F.G., and Brulis, V.J., "Perfect Chirped Echelle Grating Wavelength Multiplexor: Design and Optimization," Photonics Journal, IEEE , vol.5, no.2, pp.2400123,2400123, April (2013), doi: 10.1109/JPHOT.2013.2251874.
10. Timo Aalto, Mikko Harjanne, and Matteo Cherchi, "VTT's micron-scale silicon rib+strip waveguide platform," Proc. SPIE 9891, Silicon Photonics and Photonic Integrated Circuits V, 98911G (13 May 2016); https://doi.org/10.1117/12.2234588
11. Janz, A. Balakrishnan, S. Charbonneau, P. Cheben, M. Cloutier, A. Delâge, K. Dossou, L. Erickson, M. Gao, P. A. Krug, B. Lamontagne, M. Packirisami, M. Pearson, and D.-X. Xu "Planar waveguide echelle gratings in silica-on-silicon," in IEEE Photonics Technology Letters, vol. 16, no. 2, pp. 503-505, Feb. 2004, doi: 10.1109/LPT.2003.823139.